International Journal of Numerical Methods
for Calculation and Design in Engineering

ARTICLE

Computational Framework for AI-IoT Integration in Brain Tumor Detection: Numerical Modeling, Algorithmic Optimization and Real-Time Deployment

Franklin Ndah Tah[1,*], Misbahu Koramar Boko Lawal[2], Abdullahi Umar Ibrahim[1,3], Suleyman Asir[1], Pwadubashiyi Coston Pwavodi[2], Chidi Wilson Nwekwo[1], Serife Kaba[1] and Basil Barth Duwa[1]

[1]Department of Biomedical Engineering, Near East University, Near East Boulevard, ZIP: 99138Nicosia, North Cyprus, via Mersin 10, Turkey
[2]Department of Bioengineering/Biomedical/Medical Engineering, Faculty of Engineering, Cyprus International University, Haspolat, Nicosia, Cyprus, Turkey
[3]Department of Medical Biochemistry, Kaduna State University, Kaduna, Nigeria
*Corresponding Author: Franklin Ndah Tah. Email: franklin.ndahtah@neu.edu.tr

Received: 05 February 2026; Accepted: 20 April 2026

ABSTRACT: The integration of Artificial Intelligence (AI) and the Internet of Medical Things (IoMT) presents significant computational and engineering challenges, especially in the deployment of real-time diagnostic systems. Therefore, this study proposed a numerically optimized and computationally efficient framework that combines deep learning (DL) architectures with IoMT-enabled deployment for the automated detection and classification of brain tumors using Magnetic Resonance Imaging (MRI). The methodology revolves around rigorous numerical preprocessing techniques, including normalized resizing, advanced data augmentation, and computationally efficient feature extraction via both custom and pre-trained Convolutional Neural Networks (CNNs). The key contributions of this study are tailored toward the evaluation of algorithmic performance beyond diagnostic accuracy, incorporating metrics such as model convergence, inference latency, memory footprint, and numerical stability under varied input conditions. The proposed AI-IoMT framework, known as I-BRAINDETECT, implemented as a web-based IoMT platform, demonstrates how algorithmic design and computational modeling can address the limitations of real-time medical image analysis. Performance evaluation and comparative analysis have shown that EfficientNetB0 and DenseNet121 achieved optimal performance in binary classification with 98.5 ± 0.202% accuracy, while ResNet50 excelled in multiclass classification with 95.4 ± 1.01% accuracy, both within a computationally constrained IoT environment. Validation of the trained models on an external dataset (Figshare) has shown that DenseNet121 achieved the best result with 93.99% accuracy. This work underscores the necessity of numerical robustness and algorithmic efficiency in bridging AI and IoT for scalable biomedical engineering solutions.

KEYWORDS: Brain tumor; magnetic resonance imaging (MRI); deep learning; computer-aided detection (CAD); internet of things (IoT)

1 Introduction

The brain is regarded as the most complex and vital organ responsible for carrying out important functions, including autonomous and voluntary activities. Thus, brain malfunction due to disease, injury, or accident can lead to impairment. Among the most severe diseases affecting the brain is a brain tumor [1]. Brain tumors are considered one of the deadliest and most fatal diseases due to their location. Brain tumors can be described as the abnormal growth of brain cells, which can cause severe impairment of brain function and even death. The general symptoms of a brain tumor include headaches, dizziness, nausea, poor vision and hearing, seizures, etc. Both primary and secondary central nervous system (CNS) tumors exert a significant burden on the global healthcare sector, accounting for over 250,000 cases annually. Over 80,000

cases of malignant and non-malignant CNS tumors were reported in the US alone in 2022 [2]. According to Cancer statistics, brain tumors are ranked as the 10th leading cause of mortality globally [3].

Brain tumors can be divided into benign and malignant types. Benign tumors can be described as the type that does not spread to other tissues or organs, while malignant brain tumors are the ones that can spread to other tissues and organs [4]. Moreover, brain cancer can be divided based on histology and molecular features from low to higher grades, including grades I, II, III, and IV. This classification is later updated by the WHO based on molecular pathogenesis into glioma (adult and pediatric), meningioma, glioneuronal tumors, and neuronal tumors [5–7].

Early, robust, and precise detection of brain tumors is crucial for proper treatment and increases the chance of long-term survival [8]. Over the years, medical experts have developed several conventional techniques for the assessment of patients suspected of having a brain tumor. The evaluation starts with physical examination, followed by neuroimaging, biopsy, pathological examination, and molecular analysis of extracted tissues. Some of the neuroimaging techniques include Magnetic Resonance Imaging (MRI), Computed Tomography (CT), Magnetoencephalography (MEG), and Positron Emission Tomography (PET) [9]. Among these techniques, MRI is the most common technique employed by medical experts due to its ability to discriminate between structures and tissue based on contrast levels. Despite the reliance of the MRI approach due to its noninvasive nature, the 3D imaging technique and its ability to detect anomalies in soft tissues effectively, several drawbacks hinder the method [9,10]. One of the major limitations of MRI revolves around manual interpretation, which is tedious and prone to error [9].

The rapid advancement in computer science and engineering has opened new frontiers in biomedical diagnostics, capable of fostering automation, real-time monitoring, tracking, and detection of diseases [11,12]. Despite the progress achieved in the last decade, the engineering foundations such as numerical stability, algorithmic efficiency, and scalable deployment, remain underexplored in clinical literature [13–15]. While deep learning (DL) models have demonstrated remarkable diagnostic accuracy, their transition to real-time, IoT-enabled clinical environments is hampered by several limitations, including computational inefficiencies, model volatility, and a lack of integrated numerical frameworks [16–18].

In line with this, scientists refocus their attention toward the deployment of AI and its subsidiaries (of deep learning (DL) algorithms such as Artificial Neural Networks (ANNs) and Convolutional Neural Networks (CNNs). Numerous studies have demonstrated the prowess of AI-based models for the accurate discrimination between brain tumors and no-tumor [19–23] and subclasses of brain tumors such as glioma, meningioma, and pituitary [24–28].

Beyond traditional CNN architectures, recent studies have turned their attention toward Transformer-based models that capture both global and local features through self-attention mechanisms. This innovation has been shown to address the inherent limitation of CNNs in modeling long-range spatial dependencies in brain MRI [29]. Complementing architectural innovations, optimal feature extraction strategies have proven crucial for maximizing diagnostic performance from medical images [30]. Despite the considerable number of studies on this topic, the majority of existing studies are limited by the deployment of pre-trained CNNs, binary classification, offline detection, and often lack computational performance and numerical stability analysis.

This study addresses these engineering gaps by proposing a computationally grounded pipeline for brain tumor detection from MRI scans. Unlike prior works that focus predominantly on clinical outcomes, this study emphasizes the numerical algorithms, pre-processing methodologies, and computational architectures that underpin a reliable AI-IoT system. The main contribution of this study is enumerated below:

- Binary classification of MRIs into tumor and non-tumor.
- Quaternary classification of MRIs into glioma, meningioma, pituitary, and no tumor.
- Development of a CAD/IoMT-based platform for real-time detection and classification of brain tumors and non-tumors.

- A comprehensive numerical stability analysis under noisy conditions simulating real-world IoMT deployment.
- Systematic evaluation of computational performance metrics (inference latency, memory footprint) is critical for edge deployment.
- Integration of these numerical considerations into a deployable IoMT framework (I-BRAINDETECT) that balances accuracy with computational constraints.

2 Methods

The overall framework of this study revolves around data curation, numerical pre-processing and augmentation and the deployment of customized (or untrained) CNN models and five pre-trained models, including DenseNet121, EfficientNetB0, ResNet-18, ResNet-50 and MobileNetV2 for the 2-way and 4-way classification of brain tumors. The performance of the models is evaluated based on accuracy, recall, precision, F1 score and AUC. The overall experimental setup is illustrated in Fig. 1.

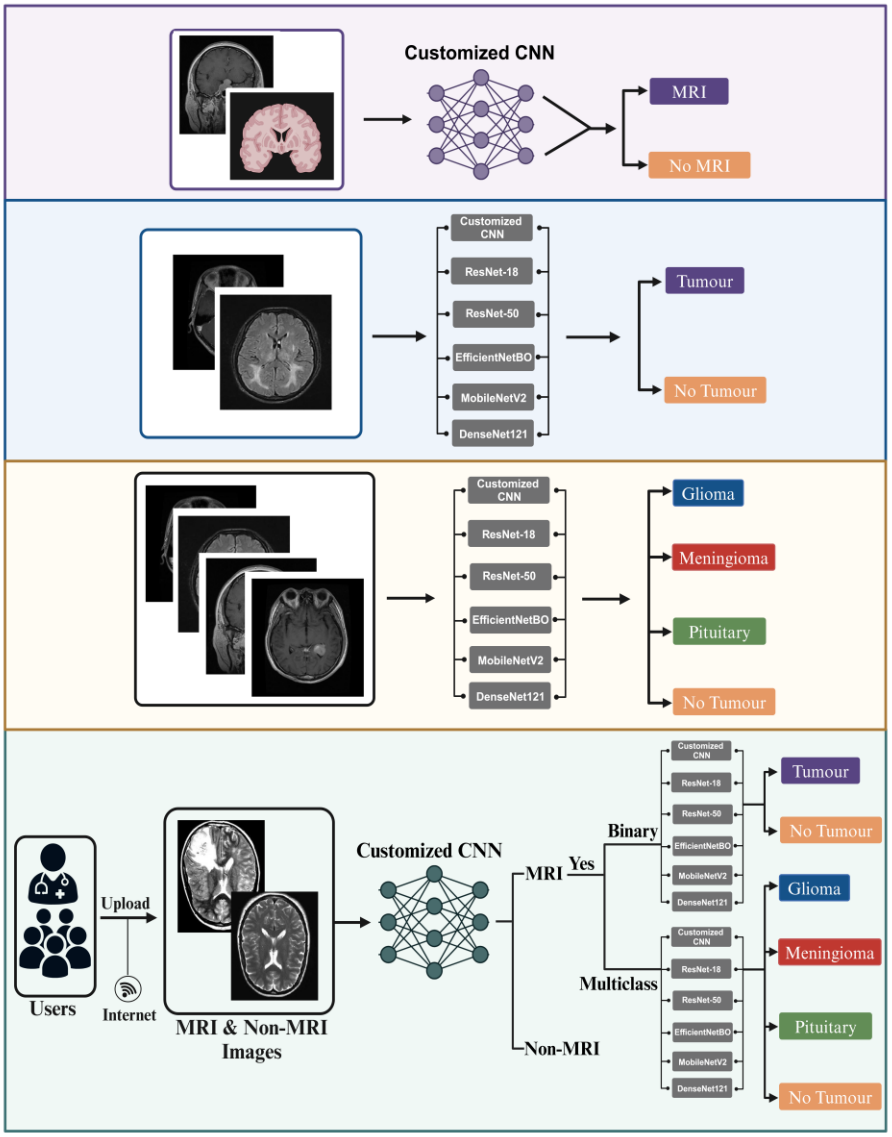

Figure 1: Overview of the proposed experimental framework, from data preprocessing to model deployment.

2.1 Data Collection

To train our models to accurately discriminate between binary classes of tumor vs. no tumor and quaternary classes such as pituitary, meningioma, glioma and no tumor, we curated 2 datasets from the Kaggle repository.

Brain Tumor Detection MRI (BTD-MRI)

The BTD-MRI dataset comprises 3060 total MRIs: 1500 tumors and 1500 non-tumors for training/validation, with 60 additional images for testing arranged in three subfolders. However, we only use 3000 images. The dataset is accessible through this website: https://www.kaggle.com/datasets/abhranta/brain-tumor-detection-mri. The summary of the dataset based on several images and composition is presented in Table 1. The samples of each class are presented in Fig. 2.

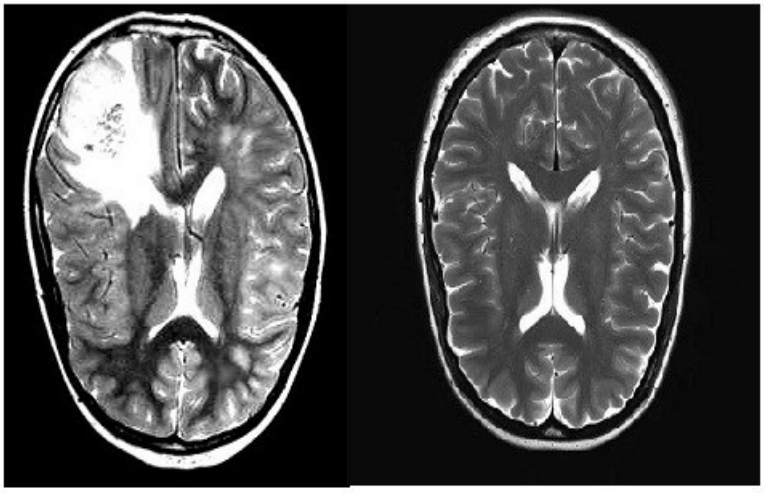

Figure 2: Samples of the BTD-MRI dataset. Left: Benign. Right: Malignant.

Table 1: Description of BTD-MRI dataset.

Classes	Number of images	%
Tumor	1500	50
No tumor	1500	50

The BMS-BTC dataset comprises 1311 brain tumor MRI scans belonging to four classes: pituitary (300 images), meningioma (306 images), glioma (300 images), and no tumor (405 images). The dataset is accessible through this website: https://www.kaggle.com/datasets/shreyag1103/brain-mri-scans-for-brain-tumor-classification. The summary of the dataset based on several images and composition, samples of the BMS-BTC dataset are presented in Table 2, and Fig. 3, respectively.

Table 2: Description of the BMS-BTC dataset.

Classes	Number of images	%
Pituitary	300	22.88
Meningioma	306	23.34
Glioma	300	22.88
No tumor	405	30.89

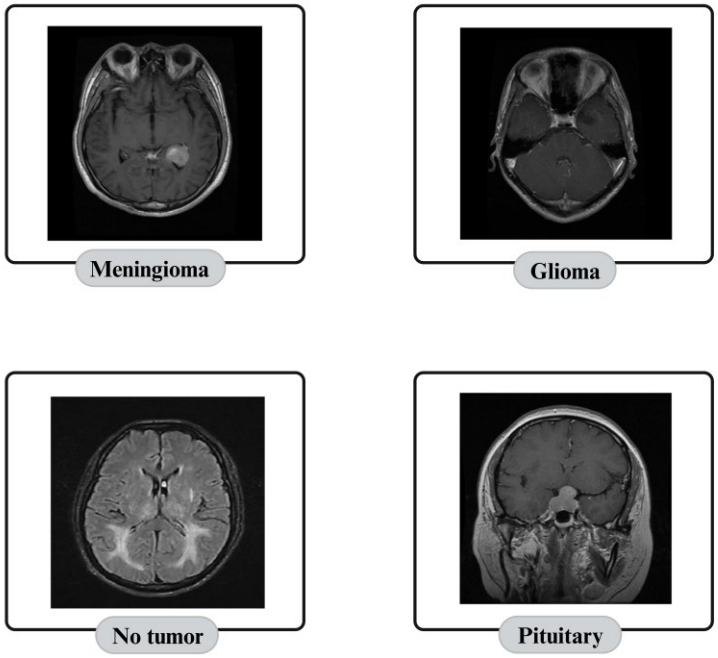

Figure 3: Samples of the BMS-BTC dataset.

2.2 Data Split

The dataset used for the binary classification comprises 3000 images. The images were already pre-split into training and testing sets. We kept this ratio of 600 images in the test set and 2400 in the training set. Using flow generators in TensorFlow from the training set, we set aside 40% of the images for validation, resulting in 1440 for testing and 960 for validation. The multiclass classification dataset went through similar splitting and data augmentation processes. The dataset comprises 1314 images, pre-split between 198 for testing and 1112 for training. A flow generator was used from the training set to obtained a split for the validation set. Considering the limitations of the dataset in terms of volume, the split is reduced from 40% to 20%, resulting in new values for training (889 images) and validation (223 images).

2.3 Numerical Preprocessing and Augmentation

To ensure model robustness and numerical stability, a multi-stage preprocessing pipeline was implemented. All MRI images were normalized to a [0, 1] range using min-max scaling to reduce variance and accelerate gradient convergence. Images were resized to 224 × 224 pixels using bilinear interpolation, chosen for its computational efficiency and minimal artifact introduction. These preprocessing techniques helped the models generalize and perform well on the unseen set and some random test images online. To improve generalization, and produce a more robust model, an offline data augmentation was carried out on the training set only. The process was carried out using Keras image generator and incorporated the following transformations:

rotation_range = 20,
width_shift_range = 0.1,
height_shift_range = 0.1,
shear_range = 0.1,
zoom_range = 0.2,

horizontal_flip = True,

vertical_flip = False,

brightness_range = [0.8, 1.2],

fill_mode = “nearest”

These transformations were applied dynamically during training using a generator-based approach to minimize memory overhead and simulate a broader dataset distribution without storage duplication. The overall augmentation of the binary dataset increased the total training images by approximately 3 times their original value (i.e., from 1440 to approximately 4320). While for the multiclass dataset, the training set increased 4 times its value (i.e., from 889 to 3556).

2.4 Custom CNN

The Custom CNN model is designed to have very few layers and capture as much data as possible to perform prediction, but not too much that it would slow training and prediction. The main aim was to create a lightweight model suitable for environments with tight software constraints, capable of discriminating between MRI and non-MRI images quickly. This prediction is fast and only takes about 300 ms. There are three versions of the Custom CNN model, but they all stem from this first one with slight variations, including more dropout layers and regularization. The Custom CNN model that powers the MRI scan for MRI and non-MRI images is a 5-layer CNN. However, the model does not include dropout, pooling or flattening layers, as they do not add parameters to the model for training. The first layer takes in our input of 224 × 224 and connects to the second layer with half its dimensions of 112 × 112. The next layer halves the dimensions again to 56 × 56, and the following layer to 28 × 28. The final layer is then flattened and results in an output of two values: ‘MRI’ and ‘non-MRI’.

For the second Custom CNN model, which powers the prediction for the binary classifications, it is designed with six layers. It starts with 224 × 224, halving the same to 112 × 112, then 56 × 56 to 14 × 14 inputs. The progressive reduction of dimensions (i.e., from 224 × 224 to 112 × 112 to 56 × 56) was designed to exponentially increase the receptive field while reducing spatial dimensions, which enable the network to learn hierarchical features from fine details to global structures. Consequently, dropout layers (rate = 0.5) were added in order to subsequent versions to prevent overfitting due to the limited dataset size.

The next step involves flatten of all the layers, prior to connect them to an output-dense layer with two output values, ‘yes’ and ‘no’. For the last Custom CNN model that powers the prediction of the multiclass classifications, it is designed with five layers, similar to the first CNN model, but with the dropout and regularization of the second model. It starts at 224 × 224, halves itself to 112 × 112, then 56 × 56 and stops at 28 × 28. The layers are flattened and passed through a dense output node with four values, which include ‘glioma’, ‘meningioma’, ‘no tumor’ and ‘pituitary’. The detailed layers of the 3 custom CNNs are presented as Fig. S1, Fig. S2 and Fig. S3 in the supplementary file 1.

2.5 Pre-Trained Models: Rationale

This study deployed ResNet-18, ResNet-50, MobileNetV2, DenseNet121, and EfficientNetB0.

Based on the “No Free Lunch” theorem, there is no single “best” model that works optimally for every problem. An algorithm that excels at classifying natural images (e.g., ImageNet) might perform poorly on medical images (e.g., X-rays) or satellite imagery, which have different statistical properties, textures, and object scales. Therefore, the only way to find the best model for a specific task is to empirically test a diverse set of models. EfficientNetB0 is another architecture that offers a superior balance between accuracy, speed, model size, fewer parameters and lower computational demands. Moreover, EfficientNetB0 as the first variants or baseline offer faster training times, reduced energy consumption, and easier deployment on resource-constrained devices like mobiles and embedded systems due to lower depth, width, image resolution compared with B1 to B7 variants.

MobileNetV2 is selected due to its application specifically for mobile platforms. It offers a superior balance of high accuracy, significantly faster and low computational cost compared to many models such as VGG or ResNet. While newer architectures have been introduced recently, ResNet remains a highly robust, well-understood and widely used CNN for several computer application tasks such as image classification and object detection. ResNet offer an excellent balance of performance and reliability. Considering the fact that there are several variants of ResNets, ResNet50 is selected due to superior accuracy on challenging datasets and less computation than ResNet152, while ResNet18 is selected due to it low computational parameters. Consequently, DenseNet121 is deployed due to its strong characteristics, including parameter-efficient, high accuracy, and ease of training. Moreover, unlike traditional networks, where each layer learns a new set of features, often discarding or re-learning features that were already computed in earlier layers, DenseNet121 addressed this problem, where each layer receives all preceding feature maps as input, and can explicitly reuse features learned by any previous layer.

2.6 Training Parameters

Due to limited number of images in the two datasets, data augmentation was conducted to enlarge the training dataset. The custom CNN was first trained with augmented data to evaluate its performance on discriminating between MRI and non-MRIs. However, we needed deeper models that could extract more features and make predictions that are more meaningful. Rather than relying on fresh models, we utilized transfer learning. Apart from the Custom CNN model, every other model was loaded with weights from ImageNet and then tuned to the new data by training them with different epoch counts, adding more regularization and lowering the learning rate. For the study, we ended training for 15 epochs.

Since the standard input size for the majority of pre-trained models is 224 × 224, training with this resolution can be time-consuming. However, training models with this size would take hours if not days to train fully. Our approach was to write the code, test it on a base M2 Apple laptop and then fully train them on a server. The server was a powerhouse A40 GPU with 45 GB GPU memory able to output 29.9 Teraflops of power along with 64 GB RAM and 128 CPU cores.

The server had Jupyter Notebook installed, enabling us to utilize its full power over the webUI instead of using a native operating system GUI that would eat up GPU use. All models were trained, tuned and refined on the server. The models, along with their metric values and graphs, were then zipped and downloaded to a computer. This approach helped models train smoothly without consuming too much time. Even though the server was fast, most models were trained and had their hyperparameters tuned a couple of times before getting their optimum high accuracy. With fast server resources, transfer learning and flow image generators. Models were able to quickly train and learn underlying features and patterns from the training sets. After training, the models were tested using the reserve set to evaluate their performances. The overall training parameters are summarized in Table 3.

Table 3: Training Parameters.

Parameters	BTD-MRI Dataset	BMS-BTC Dataset
Optimizer	Adam	Adam
Learning Rate	0.000001	0.000001
Batch size	32	32
Epochs	35	35
Loss function	Binary crossentropy	Categorical crossentropy

2.7 Statistical Analysis

A statistical method based on Analysis of Variance ANOVA is used to assess significant differences between the means of models trained after five rounds. One-way ANOVA is computed for each classification (i.e., binary and multiclass).

Total sum of squares

$$SST = \sum_{i=1}^{k}\sum_{j=1}^{ni}(x_{ij} - \bar{x})^2 \quad (1)$$

Between-groups sum of squares

$$SSB = \sum_{i=1}^{k} ni\ (x_i - \bar{x})^2 \quad (2)$$

Within-groups sum of squares

$$SSW = \sum_{i=1}^{k}\sum_{j=1}^{ni}(x_{ij} - \bar{x}_i)^2 \quad (3)$$

Degrees of freedom

$$df_b = k - 1\ =\ 5,\ df_w = N - k = 24, \qquad df_{total} = N - 1\ =\ 29 \quad (4)$$

Mean squares

$$MSB = \frac{SSB}{df_b}, MSW = \frac{SSW}{df_w} \quad (5)$$

F-statistic

$$F = \frac{MSB}{MSW} \quad (6)$$

where $k = 6$, each with n_i observations (all $n_i = 5$), total $N = \sum n_i = 30$. x_{ij} is the j-th observation in group, $i, \bar{x}_i$ the group mean and $\bar{x}$ the overall mean.

These calculations were performed for each metric separately, using the data from the five runs of each model across the two tasks. The results of the models after five rounds are presented in supplementary file 2 for binary classification and supplementary file 3 for multiclass classification, respectively.

3 Result

The integration of AI into medical diagnosis is critical due to the exponential growth of medical data generated from diverse medical devices, the increased workload faced by medical practitioners, the likelihood of misdiagnosis etc. The implementation of DL model in medical imaging continue to transform the field into a more efficient, precise, reliable, affordable and time-saving procedure. The increase in the volume of medical data, such as textual data from digital devices, audio signals, and biomedical images, such as MRIs, X-rays, Ultrasound, CT scans, SPECT, PET or hybrids serve as fuel for training DL-based models. These wide ranges of images are use as input to trained DL-based tools for accurate classification of diseases and contribute significantly to reducing errors and high workload faced by healthcare expert. By conforming to this technique, we developed three customized CNN models from scratch and implemented five pre-trained models for the binary and multi-class classification of brain tumors. We first implemented Custom CNN to discriminate between MRI and non-MRI images, which resulted in 99.62% accuracy. The second step include training and testing of the models using 2 datasets in which the models are trained using 80% of the dataset based on 30 epochs and testing using 20% based on accuracy, sensitivity, specificity, precision, recall, and AUC or ROC curve, F1-score. The training graphs of the four best models (DenseNet121, MobileNetV2, EfficientNetB0, and Custom CNN) and (DenseNet121, MobileNetV2, EfficientNetB0, and ResNet50) deployed for binary classification and multi-class classifications are shown in Fig. 4 and Fig. 5, respectively, while the remaining graphs are presented in Fig.

S4 (ResNet18 and ResNet50), and Fig. S5 (Custom CNN and ResNet18) respectively in the supplementary file 1.

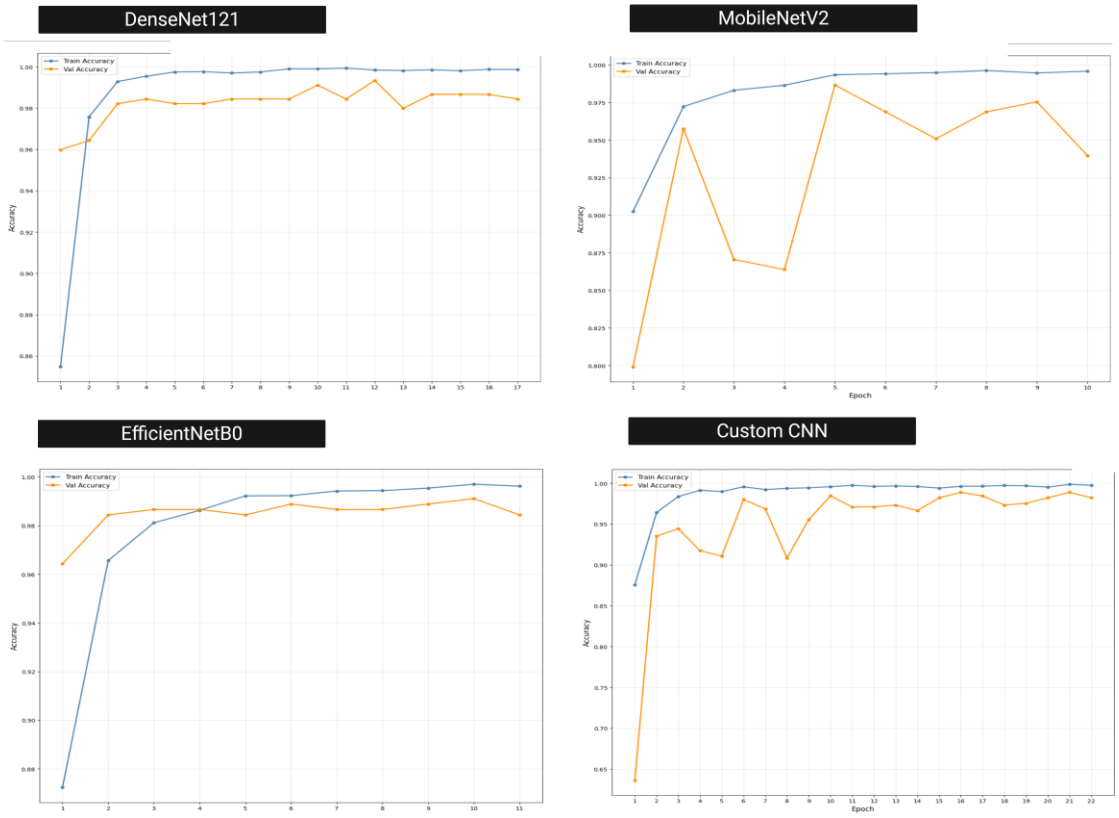

Figure 4: Training graphs of the four best models (DenseNet121, MobileNetV2, EfficientNetB0, and Custom CNN) deployed for binary classification.

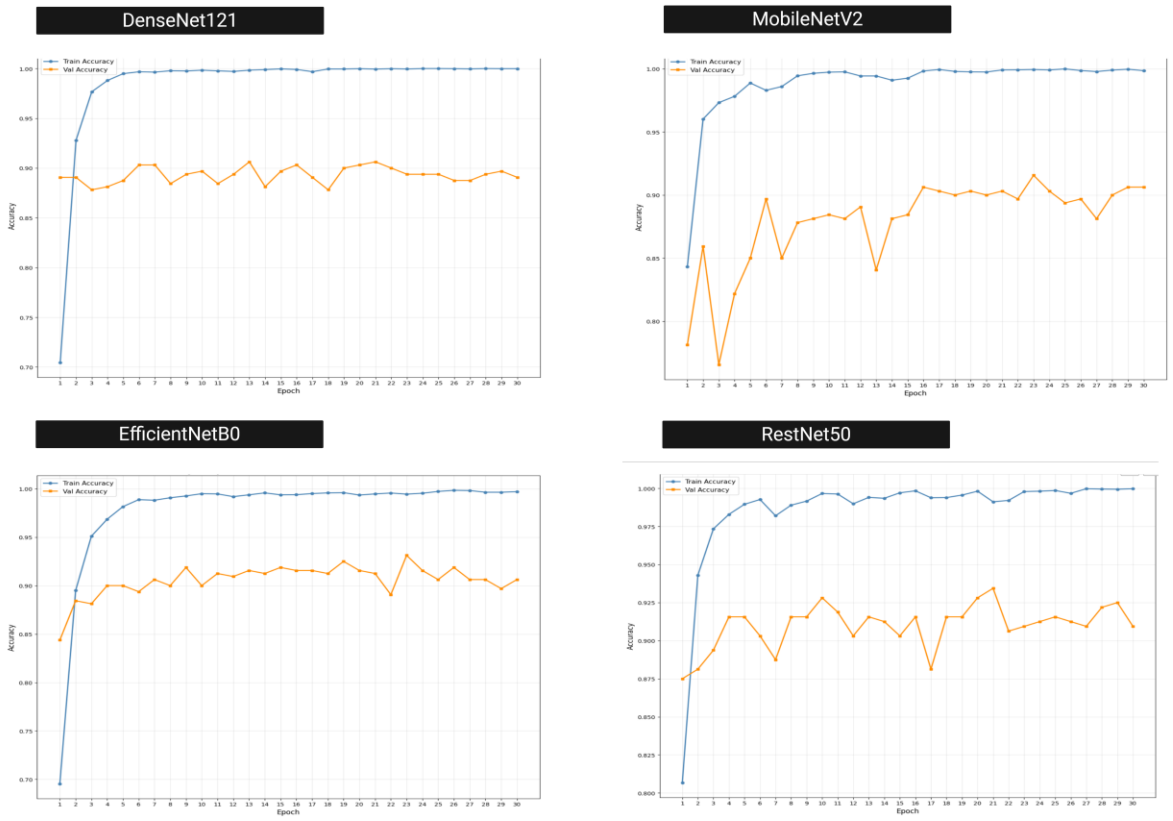

Figure 5: Training graphs of the four best models (DenseNet121, MobileNetV2, EfficientNetB0, and ResNet50) deployed for multi-class classification.

3.1 Evaluation Metrics

To evaluate the proposed frameworks, the following metrics are used: accuracy, sensitivity, specificity, precision, recall, AUC or ROC curve, and F1-score.

$$\textbf{Accuracy} = \frac{TP + TN}{FP + FN} \tag{7}$$

$$\textbf{Precision} = \frac{TP}{TP + FP} \tag{8}$$

$$\textbf{Recall} = \frac{TP}{TP + FN} \tag{9}$$

$$\textbf{Specificity} = \frac{TN}{TN + FP} \tag{10}$$

$$\textbf{F1} = \frac{Precision\ x\ Recall}{Precision + Recall} \tag{11}$$

3.2 Performance Evaluation of Models Trained and Tested for Binary Classification (BTD-MRI Dataset)

3.2.1 Testing Set

Binary classification is crucial for understanding whether suspected patients are suffering from brain tumors. However, a subsequent analysis is required to establish the tumor subtype if the patient tests positive. Both untrained and pre-trained models are trained and tested using the BTD-MRI dataset. The results are presented in in Table 4.

Table 4: Performance evaluation of models trained and tested for binary classification.

Model/Performance Metrics (%)	Accuracy	Recall	Precision	Specificity	F1-Score	AUC
Customized CNN	97.6 ± 0.841	98.0 ± 0.866	97.2 ± 1.258	97.2 ± 1.313	97.6 ± 0.826	99.5 ± 0.162
ResNet-18	97.6 ± 0.656	98.1 ± 0.912	97.2 ± 1.758	97.1 ± 1.823	97.6 ± 0.639	99.8 ± 0.12
ResNet-50	98.2 ± 0.427	97.7 ± 0.704	98.7 ± 0.373	98.7 ± 0.372	98.2 ± 0.433	99.6 ± 0.078
MobileNetV2	97.8 ± 0.614	98.8 ± 0.674	96.8 ± 1.341	96.7 ± 1.454	97.8 ± 0.591	99.6 ± 0.098
DenseNet121	98.5 ± 0.202	98.3 ± 0.491	98.7 ± 0.483	98.5 ± 0.195	98.5 ± 0.202	99.7 ± 0.137
EfficientNetB0	98.5 ± 0.202	99.2 ± 0.373	97.9 ± 0.485	97.9 ± 0.508	98.5 ± 0.196	99.9 ± 0.045

3.2.2 Confusion Matrix

For binary classification, the models were evaluated using 450 images (225 for each class). The results indicated that Custom CNN accurately classified 220 tumor cases (220/225, 97.77%) and 222 no tumor cases (222/225, 98.66%) with an overall accuracy of 98.22%. DenseNet121 accurately classified 220 tumor cases (220/225, 97.77%) and 224 no tumor cases (224/225, 99.55%) with an overall accuracy of 98.66%. EfficientNetB0 accurately classified 223 tumor cases (223/225, 99.11%) and 220 no tumor cases (220/225, 97.77%), with an overall accuracy of 98.44%. MobileNetV2 successfully classified 223 tumor cases (223/225, 99.11%) and 221 no tumor cases (221/225, 98.22%), with an overall accuracy of 98.66%. Performance evaluation of ResNet18 has shown that the model accurately classified 219 tumor cases (219/225, 97.33%) and 224 no tumor cases (224/225, 99.55%) with an overall accuracy of 98.44%. Lastly, ResNet50 accurately classified 219 tumor cases (219/225, 97.33%) and 222 no tumor cases (222/225, 98.66%) with an overall accuracy of 98.00%. The confusion matrixes of the four best models (DenseNet121, MobileNetV2, EfficientNetB0 and ResNet18 are presented in Fig. 6, while remaining two models (Custom CNN and ResNet50) are presented in Fig. S6, in the supplementary file 1.

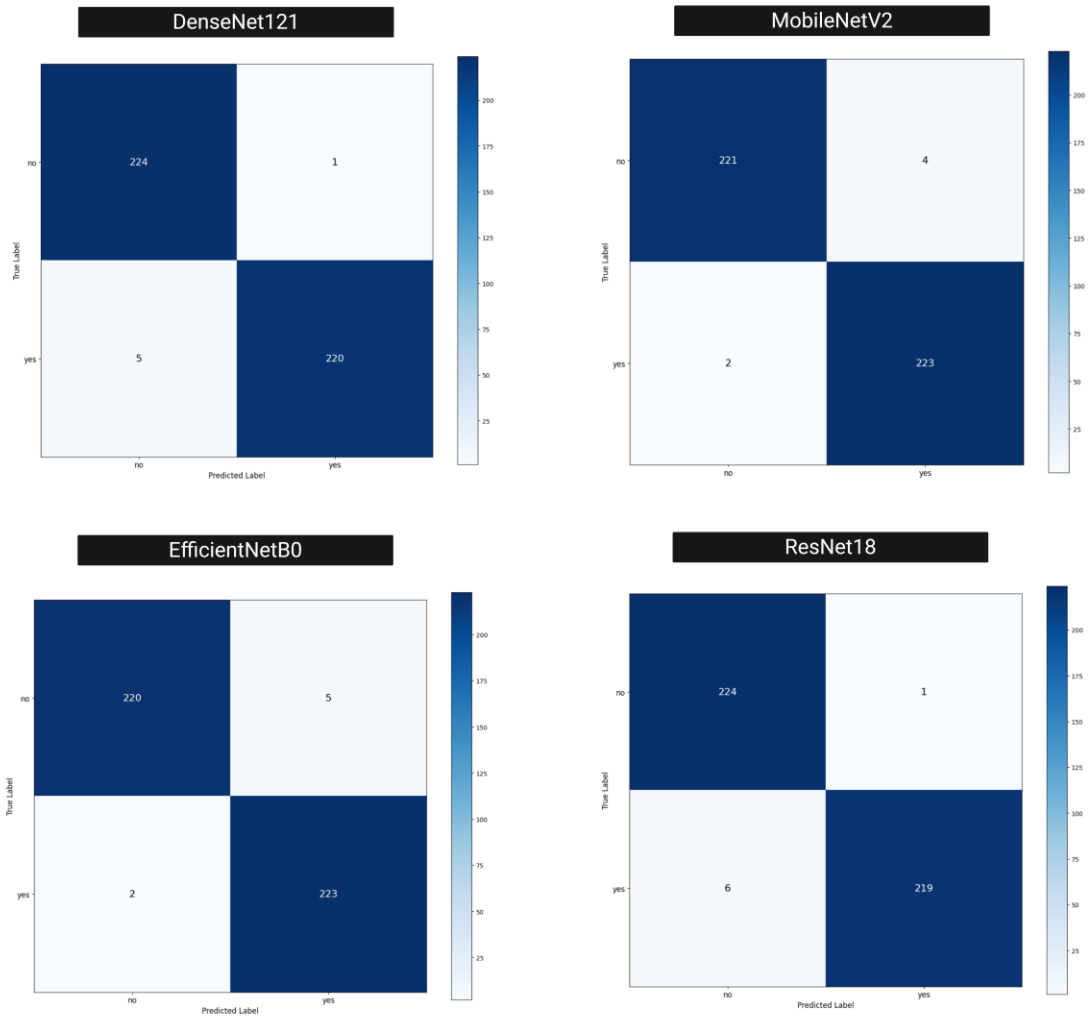

Figure 6: Confusion matrix of the four best models tested for binary classification.

3.3 Performance Evaluation of Models Trained and Tested for Multi-Class Classification (BMS-BTC Dataset)

3.3.1 Testing Set

As a result of the fact that there are several subtypes of brain tumors, training models to discriminate between these subtypes is crucial for proper treatment. Thus, in this study, untrained and pre-trained models are trained and tested using the BMS-BTC dataset. The results are presented in Table 5.

Table 5: Performance evaluation of models trained and tested for multi-class classification.

Model/Performance Metrics (%)	Accuracy	Recall	Precision	Specificity	F1-Score	AUC
Customized CNN	92.4 ± 0.946	92.5 ± 1.02	91.9 ± 1.01	97.4 ± 0.307	91.9 ± 0.997	98.9 ± 0.564
ResNet-18	89.8 ± 5.11	90.7 ± 4.25	89.2 ± 5.41	96.5 ± 1.74	89.1 ± 5.29	98.5 ± 1.04
ResNet-50	95.4 ± 1.01	96.0 ± 1.83	95.1 ± 1.03	98.4 ± 0.326	95.1 ± 1.07	99.4 ± 0.189
MobileNetV2	93.0 ± 1.80	93.1 ± 1.81	92.7 ± 1.86	97.6 ± 0.588	92.6 ± 2.01	99.1 ± 0.374
DenseNet121	94.0 ± 0.748	94.1 ± 0.885	93.7 ± 0.807	98.0 ± 0.244	93.7 ± 0.802	99.3 ± 0.199
EfficientNetB0	94.75 ± 1.46	94.6 ± 1.42	94.5 ± 1.53	98.2 ± 0.472	94.4 ± 1.61	99.4 ± 0.108

3.3.2 Confusion Matrix

For multi-class classification, the models were evaluated using 198 images for the 4 classifications, including glioma (45), meningioma (47), no tumor (61), pituitary (45). Custom CNN accurately classified 43 glioma cases (43/45, 95.55%) with 2 misclassifications, 41 meningioma cases (41/47, 87.23%) with 6 misclassifications, 61 no tumor cases (61/61, 100.00%) with 0 misclassifications and 40 pituitary cases (40/45, 88.88%) with 5 misclassifications, with an overall accuracy of 93.43%. DenseNet121 accurately classified 43 glioma cases (43/45, 95.55%) with 5 misclassifications, 39 meningioma cases (39/47, 82.97%) with 8 misclassifications, 60 no tumor cases (60/61, 98.36%) with 1 misclassification and 42 pituitary cases (42/45, 93.33%) with 3 misclassifications, with an overall accuracy of 92.92%. EfficientNetB0 accurately classified 43 glioma cases (43/45, 95.55%) with 2 misclassifications, 38 meningioma cases (38/47, 80.85%) with 9 misclassifications, 60 no tumor cases (60/61, 98.36%) with 1 misclassification and 44 pituitary cases (44/45, 97.77%) with 1 misclassification, with an overall classification accuracy of 93.43%. MobileNetV2 accurately classified 43 glioma cases (43/45, 95.55%) with 2 misclassifications, 36 meningioma cases (36/47, 76.59%) with 11 misclassifications, 61 no tumor cases (61/61, 100.00%) with 0 misclassifications and 45 pituitary cases (45/45, 100.00%) with 0 mis-classifications, with an overall classification accuracy of 93.43%.

ResNet50 accurately classified 43 glioma cases (43/45, 95.55%) with 2 misclassifications, 42 meningioma cases (42/47, 89.36%) with 5 misclassifications, 61 no tumor cases (61/61, 100.00%) with 0 misclassifications and 44 pituitary cases (44/45, 97.77%) with 1 misclassification, with an overall classification accuracy of 96.46%. ResNet18 accurately classified 40 glioma cases (40/45, 88.88%) with 5 misclassifications, 38 meningioma cases (38/47, 80.85%) with 9 misclassifications, 61 no tumor cases (61/61, 100.00%) with 0 misclassifications and 45 pituitary cases (45/45, 100.00%) with 0 mis-classifications, with an overall accuracy of 92.92%. The confusion matrixes of the four best models (ResNet50, MobileNetV2, EfficientNetB0 and Custom CNN are presented in Fig. 7, while remaining two models (ResNet18 and DenseNet121) are presented in Fig. S7, in the supplementary file 1.

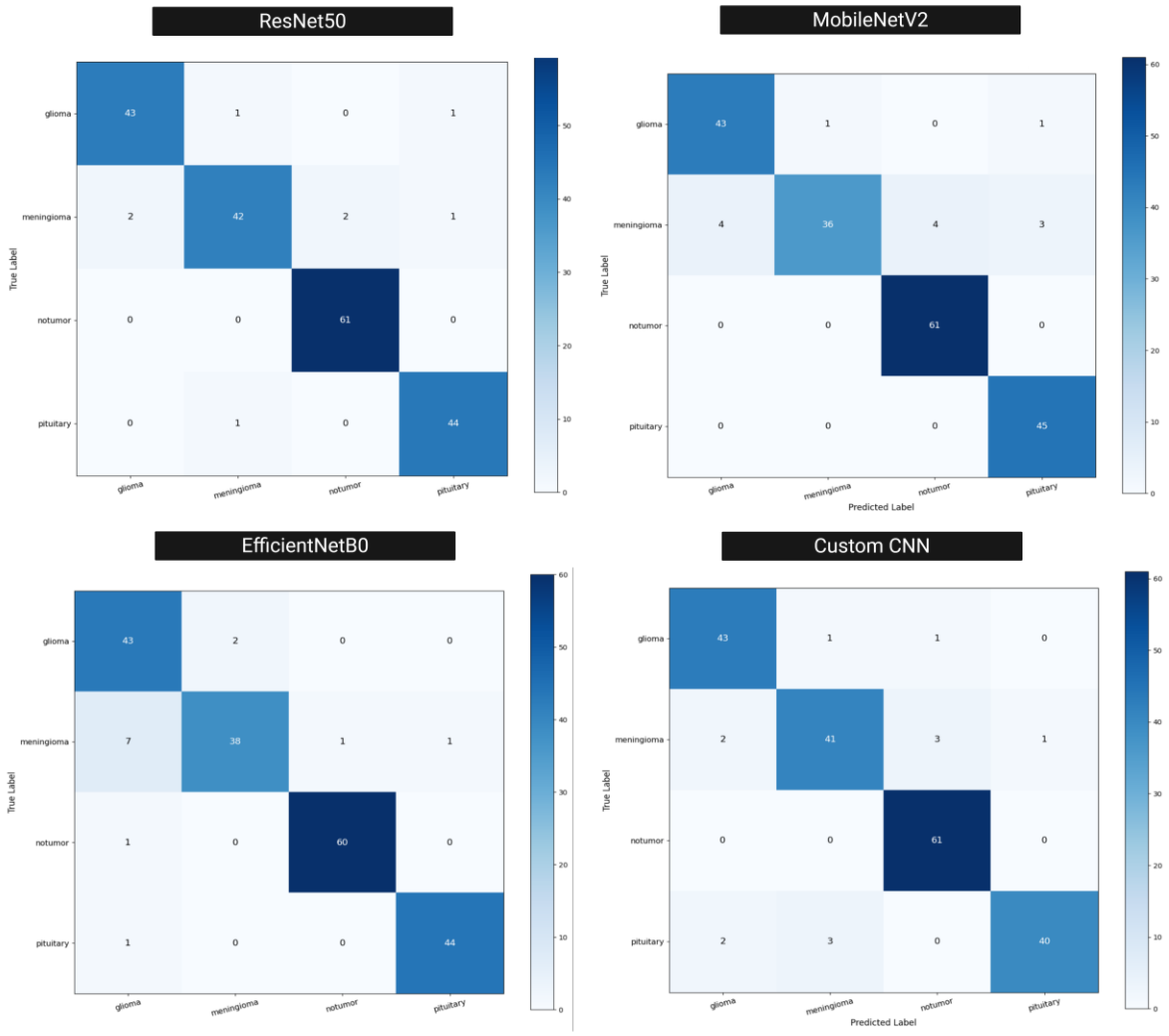

Figure 7: Confusion matrix of the best four models tested for multi-class classification.

3.4 Statistical Analysis

The ANOVA result (as shown in **Table 6**) presents the between-groups sum of squares (SSB), within-groups sum of squares (SSW), mean squares (MSB, MSW), the F-statistic, and the significance at $\alpha = 0.05$ (critical value $F_{0.05}$ (5, 24) ≈ 2.62. For binary classification, significant differences (i.e., $p < 0.05$) exist among models for accuracy, sensitivity, precision, F1 Score and ROC/AUC. Specificity do not show statistically significant differences at the 0.05 level. For multiclass classification, significant differences ($p < 0.05$) exist among models for all metrics except ROC/AUC.

Table 6: One-way ANOVA result of Binary Classification (BTD-MRI Dataset) and Multiclass Classification (BMS-BTC Dataset).

Binary Classification (BTD-MRI Dataset)							
Metric	**SSB**	**SSW**	**MSB**	**MSW**	**F**	***p*-value**	**Significant**
Accuracy	4.667	7.114	0.9334	0.2963	3.15	<0.05	Yes
Recall	7.159	11.641	1.432	0.4850	2.95	0.033	Yes
Precision	16.42	28.310	3.285	1.1795	2.785	0.041	Yes

Specificity	16.06	30.39	3.212	1.266	2.537	0.056	No
F1-Score	4.521	6.823	0.9042	0.2845	3.18	0.024	Yes
ROC/AUC	0.4634	0.3152	0.0927	0.01308	7.088	<0.01	Yes
Multiclass Classification (BMS-BTC Dataset)							
Metric	**SSB**	**SSW**	**MSB**	**MSW**	**F**	***p*-value**	**Significant**
Accuracy	101.76	135.62	20.352	5.651	3.60	0.015	Yes
Recall	115.52	151.20	23.104	6.300	3.667	0.014	Yes
Precision	85.00	114.11	17.000	4.755	3.575	0.015	Yes
Specificity	11.60	15.42	2.321	0.6427	3.61	0.015	Yes
F1-Score	114.86	149.49	22.971	6.229	3.688	0.013	Yes
ROC/AUC	3.194	6.488	0.6388	0.2703	2.363	0.072	No

3.5 Validation on Figshare Dataset

Moreover, the deployed models are validated on Figshare dataset, which contains 3064 T1-weighted contrast MRI slices distributed into three classes, including 1426 glioma, 930 pituitary tumor and 708 meningioma. The result has shown that DenseNet121 achieved the best result with 93.99% accuracy, 93.03% recall, 93.56% precision, 97.01% specificity, 93.27% F1-Score, and 99.02% ROC/AUC. Trailing behind, are MobileNet (93.67% accuracy), and ResNet50 (93.44% accuracy). The results of the deployed models on Figshare dataset are presented in Supplementary file 4.

3.6 Deployment of Model

The proposed AI/IoT-enabled framework is an integrated system deployed online at (https://braintumourapp-a9dtj6qqinnjjcpgrddrvo.streamlit.app/). The system is designed to processes any uploaded image in two phases. Phase one is characterized based on discrimination between MRI vs. Non-MRI. If the uploaded image is not an MRI image, the processing pipeline ends. However, if the uploaded image is classified in the first phase as an MRI, it automatically triggers the second phase which is classification into one of four classes (glioma, meningioma, no tumor and pituitary). The detection process revolves around 4 main steps: log in, uploading of image, selection of diagnosis and detection. The first step allows users to log in using a username and a password. The second step involves uploading an image using a viable internet connection, where the image can undergo pre-processing through resizing to fit the network input size. The next step requires diagnosis selection and subsequent binary classification in seconds and finally the multiclassification. The whole process (from upload to classification) can be achieved in less than a minute (i.e., inference time of <1 s). The step-by-step process is illustrated in Fig. 8, and a video is submitted as a supplementary file 5.

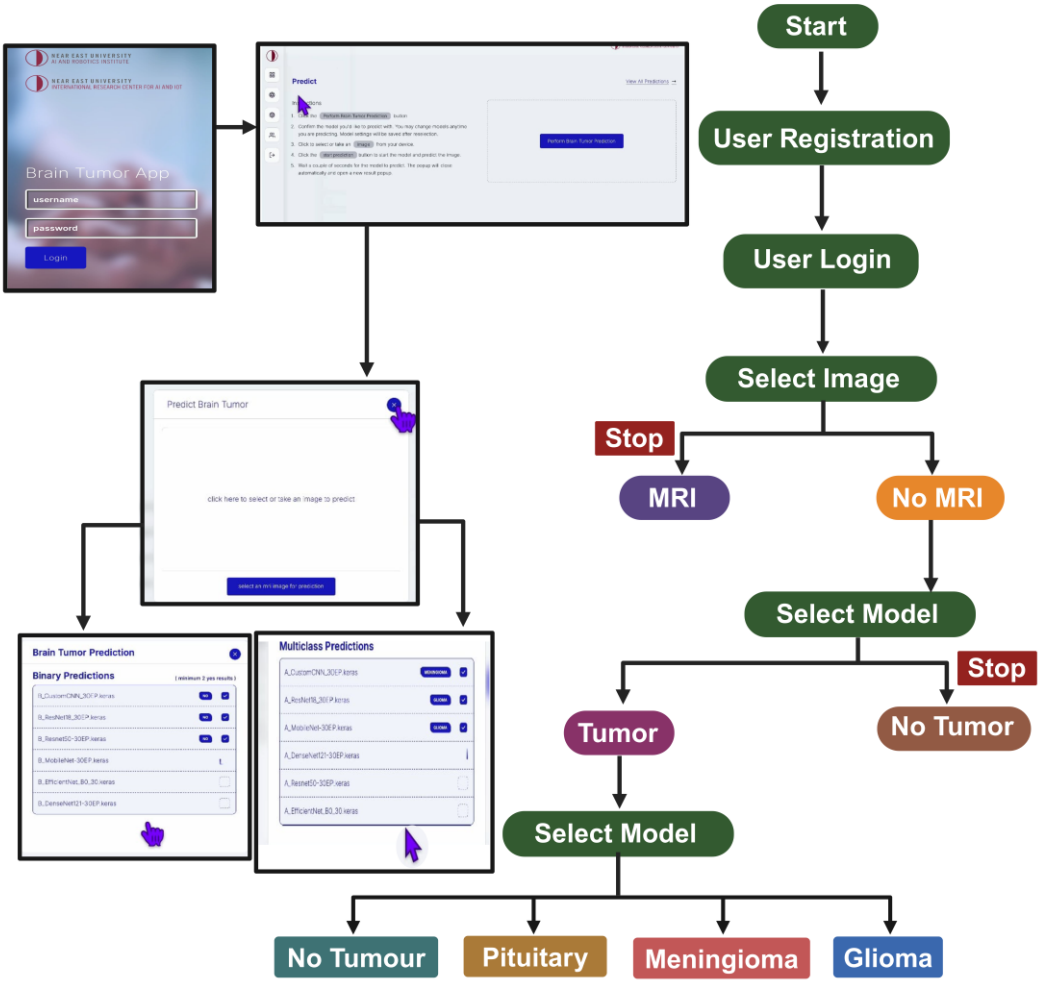

Figure 8: Deployment of CAD/IoMT framework.

3.7 Computational Performance Metrics

Aside from conventional diagnostic accuracy, recall, precision, Av. specificity, F1-Score and AUC score, models were evaluated on computational performance (convergence analysis and theoretical model complexity), critical for IoT deployment. These metrics were recorded during the inference phase for each task as shown in Table 7. The result revealed that all pre-trained models converged reliably within 12–25 epochs for binary classification. On the contrary, for multiclass classification, all pre-trained models converged reliably within 12–25 epochs except the custom CNN. The failure of Custom CNN on the multiclass task confirms that shallow architectures lack the capacity to capture the intricate features needed for 4-way classification. Consequently, owing to its lightweight characteristics, MobileNetV2 offered the best balance of speed and low memory footprint for both tasks, making it highly suitable for edge deployment. ResNet-18 on the other hand, provided a strong compromise between accuracy, speed and convergence stability across both classifications. In contrast, deeper models (such as ResNet-50, DenseNet121) incurred higher latency and memory costs. Consequently, the measured inference times correlate well with theoretical FLOPs: MobileNetV2, the fastest with 0.3 GFLOPs, while DenseNet121 with 2.9 GFLOPs and ResNet-50 with 3.8 GFLOPs are slower.

Table 7: Computational Performance for Binary Classification (BTD-MRI Dataset) and Multiclass Classification (BMS-BTC Dataset).

Binary Classification (BTD-MRI Dataset)					
Models	**Avg. Inference Time (ms)**	**Memory Footprint (MB)**	**Parameters**	**FLOPs (G)**	**Training Convergence (Epochs to 99% Val Acc)**
Custom CNN	18	12	0.5	0.1	22
ResNet-18	45	89	11.7	1.8	12
ResNet-50	62	145	25.6	3.8	15
MobileNetV2	32	64	3.4	0.3	18
DenseNet121	78	210	8.0	2.9	20
EfficientNetB0	55	104	5.3	0.4	16
Multiclass Classification (BMS-BTC Dataset)					
Models	**Avg. Inference Time (ms)**	**Memory Footprint (MB)**	**Parameters**		**Training Convergence (Epochs to 99% Val Acc)**
Custom CNN	22	15	0.5	0.1	N/A
ResNet-18	48	89	11.7	1.8	14
ResNet-50	65	145	25.6	3.8	18
MobileNetV2	35	64	3.4	0.3	20
DenseNet121	81	210	8.0	2.9	25
EfficientNetB0	58	104	5.3	0.4	22

3.8 Numerical Stability Analysis

In order to assess model robustness and reliability in real-world IoMT scenarios where input quality may vary, a numerical stability test was conducted. This analysis is imperative for IoMT deployment, as it highlights which models are more likely to maintain performance under suboptimal imaging conditions (e.g., sensor noise, compression artifacts). Gaussian noise ($\sigma = 0.05$) was systematically added to the test images, and the degradation in classification accuracy was subsequently measured. The rationale behind the choice of $\sigma = 0.05$ is supported by [31], which uses σ values of 5–35, with pixel intensities ranging 0–255 (8-bit) or 0–4095 (12-bit). However, in this study, the images are normalized to [0, 1], where $\sigma = 0.05$ is equivalent to $\sigma = 12.75$ on a 0–255 scale. The result of the analysis indicated that ResNet-18 demonstrated the best overall stability for binary classification resulting in the smallest accuracy drop of 2.33%. MobileNetV2 demonstrated the greatest robustness for the multiclass task, with only a 3.73% drop. While, the Custom CNN was remarkably less stable, especially for multiclass classification, indicating its simpler architecture is more sensitive to input perturbations. The summary of the numerical stability analysis for binary and multiclass classifications are presented in Table 8, respectively.

Table 8: Numerical Stability for Binary Classification (BTD-MRI Dataset) and Multiclass Classification (BMS-BTC Dataset).

Binary Classification (BTD-MRI Dataset)			
Models	**Original Test Accuracy (%)**	**Accuracy with Noise (%)**	**Accuracy Drop (%)**
Custom CNN	97.6	95.23	2.37
ResNet-18	97.6	95.27	2.33
ResNet-50	98.2	94.03	4.17
MobileNetV2	97.8	94.9	2.90
DenseNet121	98.5	95.35	3.15
EfficientNetB0	98.5	95.66	2.84
Multiclass Classification (BMS-BTC Dataset)			
Models	**Original Test Accuracy (%)**	**Accuracy with Noise (%)**	**Accuracy Drop (%)**
Custom CNN	92.4	86.24	6.16
ResNet-18	89.8	85.53	4.27
ResNet-50	95.4	89.93	5.47
MobileNetV2	93.0	89.27	3.73
DenseNet121	94.0	88.52	5.48
EfficientNetB0	94.75	89.87	4.88

3.9 Discussion

The advancement in medical technologies is facilitated by the integration of cutting-edge technologies, which include AI, big biomedical data, cloud computing, IoT etc. These technologies have been shown to aid clinicians in accurate and precise diagnosis, treatment, and analysis of electronic health records (EHRs) [30,31]. One clinical field that benefits from these technologies revolves around computer-vision-based biomedical imaging applications [31]. An AI-driven framework has been developed for the CAD of several diseases using various biomedical images, including CT, MRI, ultrasound, X-ray, etc. Integrating CAD into clinical diagnosis has improved accuracy, reduced errors, decreased workload, and saved time. Moreover, integrating IoT into CAD enables real-time infection screening, sharing of biomedical data, and monitoring and surveillance of diseases [32,33]. Thus, in this study, we proposed a framework that employs AI and IoT to augment the capabilities of neuro-oncologists/radiation-oncologists and accessible to patients for real-time and fast screening of brain cancer from MRI.

By leveraging the power of DL models, both untrained and pre-trained CNNs integrated with IoMT were deployed to create a fast and real-time platform for the binary and quaternary classification of brain tumors and non-tumors. As shown in Table 4, the result indicated that EfficientNetB0 achieved the best overall result 4/6 metrics, including accuracy (tied with DenseNet121), recall F1-score and AUC. Other noticeable models with nearly perfect score includes DenseNet (2/6), ResNet50 (1/6) and MobileNetV2. Moreover, based on the confusion matrix result, DenseNet121 and MobileNetV2 outperformed EfficientNetB0, with an overall accuracy of 98.66% (i.e., 444/450 accurate classifications and 6 misclassifications. Both EfficientNetB0 and ResNet18 trailed slightly behind, with an overall accuracy of 98.44% (i.e., 443/450 accurate classifications and 7 misclassifications, as shown in Fig. 6. Comparison between untrained custom CNN and pre-trained models has shown that the gap between these models is very narrow. Therefore, despite the limitation of custom CNN, it achieved moderate results for the binary classification of brain tumors and non-tumors.

Subsequently, the comparison of the models trained for quaternary classification has shown that ResNet50 achieved the best result across all the metrics, as shown in Table 5. EfficientNetB0 and DenseNet121 also perform very well with high scores across all metrics. Moreover, evaluation of the model using 198 has shown that ResNet50 achieved the highest score with an overall accuracy of 96.46% (i.e., 190 accurate classification and 8 misclassifications as shown in Fig. 7. On the other hand, the customized model only outperformed ResNet18 across all the 6 metrics. In comparison with the remaining pre-trained models, untrained custom CNN achieved significantly lower accuracy, precision, recall and F1-score scores, with only a significant result in average specificity and AUC. Unlike in binary classification, where the

model performs decently, therefore, increasing several classes reduces performance. The performance of both ResNet-18 and MobileNetV2 for the two tasks was also solidified in the numerical stability analysis (where Gaussian noise ($\sigma = 0.05$) was systematically added to the test images) as shown in Table 8.

3.10 Limitation and Future Outlook

DL model requires large training data to achieve optimal performance. Although using pre-trained models has achieved higher performance than untrained models, training pre-trained models with a substantial dataset can lead to high performance. One of our study's limitations includes using a small dataset acquired from Kaggle, which comprises of 3000 for binary classes and 1311 for multi-class. While publicly available from Kaggle, these two datasets may not fully represent the diversity of real-world clinical populations in terms of demographics, scanner manufacturers, and imaging protocols. Another limitation includes using single models designed using SoftMax as a classifier.

Due to the likelihood of misclassification, our future work will attempt to improve the binary classification by merging the 3 tumors (glioma, meningioma and pituitary) of the BMS-BTC dataset into a tumor. In contrast, the non-tumor will be merged with the no-tumor class of the BTD-MRI dataset. Secondly, we can improve the models' performance by acquiring more datasets such as the CE-MRI Figshare, 2020-BRATS, BD-Brain-Tumor, etc. Moreover, we will implement more data augmentation techniques such as flipping, rotation, mirroring, scaling, cropping, etc., to maximize the training set. Notwithstanding, the overall classification efficacy can be improved by exploring ML classifiers such as SVM, KNN, RF, DT etc. Another limitation of this study includes adding only $\sigma = 0.05$ Gaussian noise; therefore, future studies will extend $\sigma = \{0.0196, 0.0392, 0.0588, 0.0784, 0.0980, 0.1176, 0.1373\}$ normalized to [0, 1] or {5, 10, 15, 20, 25, 30, 35} based on 8-bit images (i.e., 0–255).

4 Conclusion

Medical practitioners use several techniques to assess a patient harboring a brain tumor. Among these techniques, the neuroimaging-based MRI approach remains the most popular and sought-after technique for screening of patients suspected of having a brain tumor. However, despite reliance on this approach, it is prone to errors due to manual interpretation, which may lead to patient morbidity and mortality. In this study, we present a computationally oriented framework for integrating DL with IoMT to enable real-time brain tumor detection. By prioritizing numerical preprocessing, algorithmic efficiency, and system-level deployment modeling, we bridge the gap between diagnostic AI and clinical IoT implementation. The overall framework revolves around the implementation of a single untrained customized model and 5 pre-trained models, which include ResNet-18, ResNet-50, EfficientNetB0, MobileNetV2, and DenseNet121 for the binary (tumor vs. non-tumor) and quaternary detection of brain tumor (pituitary, meningioma, glioma, and no tumor). Evaluation and comparative analysis between the models showed promising results while accurately discriminating between tumor and non-tumor and subclasses of brain tumors. Among the implemented models, EfficientNetB0 and DenseNet121 demonstrated a remarkable result for binary classification. While ResNet50 achieved the best result for multiclass classification. By developing a CAD/IoMT-based platform, this study aims to provide medical practitioners with an easy-to-use, fast, and reliable avenue for discriminating between brain tumors and their subclasses. The findings of this study underscore that model selection must balance accuracy with computational performance to achieve scalable and real-time diagnostic solutions. Despite the excellent result, further investigation and testing of other single, hybrid, and ensemble models are essential for improving performance. Moreover, acquiring other datasets is crucial for inclusiveness and diversification.

Acknowledgement: Not applicable.

Funding Statement: The authors received no specific funding for this study.

Author Contributions: Conceptualization, Misbahu Koramar Boko Lawal, Abdullahi Umar Ibrahim and Pwadubashiyi Coston Pwavodi; methodology, Franklin Ndah Tah, Misbahu Koramar Boko Lawal, and Suleyman Asir; data curation, Franklin Ndah Tah, Basil Barth Duwa and Suleyman Asir; writing—review and editing, Franklin Ndah Tah, Chidi Wilson Nwekwo, Serife Kaba; supervision, Abdullahi Umar Ibrahim and Pwadubashiyi Coston Pwavodi. All authors reviewed and approved the final version of the manuscript.

Availability of Data and Materials: The data that support the findings of this study are openly available in [Kaggle repository] at [https://www.kaggle.com/datasets/abhranta/brain-tumor-detection-mri], [https://www.kaggle.com/datasets/shreyag1103/brain-mri-scans-for-brain-tumor-classification] and [https://www.kaggle.com/datasets/ashkhagan/figshare-brain-tumor-dataset].

Ethics Approval: Not applicable.

Conflicts of Interest: The authors declare no conflicts of interest.

Supplementary Materials: The supplementary files “1-5” are attached. The supplementary material is available online at.

References

1. Bockaert J, Marin P. mTOR in brain physiology and pathologies. Physiol Rev. 2015;95(4):1157–87. doi:10.1152/physrev.00038.2014.
2. Zedde M, Napoli M, Moratti C, Pavone C, Bonacini L, Di Cecco G, et al. Tumor-like lesions in primary angiitis of the central nervous system: the role of magnetic resonance imaging in differential diagnosis. Diagnostics. 2024;14(6):618. doi:10.3390/diagnostics14060618.
3. American cancer society medical and editorial content team. Key statistics for brain and spinal cord tumors. [cited 2026 Jan 1]. Available from: https://www.cancer.org/cancer/types/brain-spinal-cord-tumors-adults/about/key-statistics.html
4. NCI Dictionaries. Cancer terms and definition of tumor. [cited 2026 Jan 1]. Available from: https://www.cancer.gov/publications/dictionaries/cancer-terms/def/tumor.
5. Louis DN, Perry A, Wesseling P, Brat DJ, Cree IA, Figarella-Branger D, et al. The 2021 WHO classification of tumors of the central nervous system: a summary. Neuro Oncol. 2021;23(8):1231–51. doi:10.1093/neuonc/noab106.
6. Berger TR, Wen PY, Lang-Orsini M, Chukwueke UN. World health organization 2021 classification of central nervous system tumors and implications for therapy for adult-type gliomas: a review. JAMA Oncol. 2022;8(10):1493. doi:10.1001/jamaoncol.2022.2844.
7. Smith HL, Wadhwani N, Horbinski C. Major features of the 2021 WHO classification of CNS tumors. Neurotherapeutics. 2022;19(6):1691–704. doi:10.1007/s13311-022-01249-0.
8. Fitzgerald RC, Antoniou AC, Fruk L, Rosenfeld N. The future of early cancer detection. Nat Med. 2022;28(4):666–77. doi:10.1038/s41591-022-01746-x.
9. Nadeem MW, Al Ghamdi MA, Hussain M, Khan MA, Khan KM, Almotiri SH, et al. Brain tumor analysis empowered with deep learning: a review, taxonomy, and future challenges. Brain Sci. 2020;10(2):118. doi:10.3390/brainsci10020118.
10. Chahal PK, Pandey S, Goel S. A survey on brain tumor detection techniques for MR images. Multimed Tools Appl. 2020;79(29):21771–814. doi:10.1007/s11042-020-08898-3.
11. Yarman BS, Rathore SP. The future of AI in disease detection—a look at emerging trends and future directions in the use of AI for disease detection and diagnosis. AI Dis Detect Adv Appl. 2025:265–88. Doi: 10.1002/9781394278695. doi:10.1002/9781394278695.ch12.
12. Liao QM, Hussain W, Liao ZX, Hussain S, Jiang ZL, Zhu YH, et al. Computer-aided application in medicine and biomedicine. Int J Comput Intell Syst. 2025;18(1):221. doi:10.1007/s44196-025-00936-y.
13. Nazar M, Alam MM, Yafi E, Su’ud MM. A systematic review of human–computer interaction and explainable artificial intelligence in healthcare with artificial intelligence techniques. IEEE Access. 2021;9:153316–48. doi:10.1109/ACCESS.2021.3127881.
14. Marengo A, Santamato V. A novel machine learning-optimized framework for systematic analysis of foundation models in healthcare: comprehensive algorithm optimization with governance-driven predictive modeling. IEEE Access. 2025;13:210040–88. doi:10.1109/ACCESS.2025.3636388.
15. Sufi F. Beyond the sensor: a systematic review of AI’s role in next-generation machine health monitoring. Appl Sci. 2025;15(19):10494. doi:10.3390/app151910494.

16. Alharbe N, Almalki M. IoT-enabled healthcare transformation leveraging deep learning for advanced patient monitoring and diagnosis. Multimed Tools Appl. 2025;84(19):21331–44. doi:10.1007/s11042-024-19919-w.
17. Lawal MK, Almousa M, Ibrahim AU, Pwavodi PC, Usman AG, Aloraini B. Artificial intelligent-powered detection of breast cancer. Journal of Radiation Research and Applied Sciences. 2025;18(2):101422.doi: https://doi.org/10.1016/j.jrras.2025.101422.
18. Rani S, Kumar R, Panda BS, Kumar R, Muften NF, Abass MA, et al. Machine learning-powered smart healthcare systems in the era of big data: applications, diagnostic insights, challenges, and ethical implications. Diagnostics. 2025;15(15):1914. doi:10.3390/diagnostics15151914.
19. Zubair Rahman AMJ, Gupta M, Aarathi S, Mahesh TR, Vinoth Kumar V, Yogesh Kumaran S, et al. Advanced AI-driven approach for enhanced brain tumor detection from MRI images utilizing EfficientNetB2 with equalization and homomorphic filtering. BMC Med Inform Decis Mak. 2024;24(1):113. doi:10.1186/s12911-024-02519-x.
20. Sawant A, Bhandari M, Yadav R, Yele R, Bendale MS. Brain cancer detection from MRI: a machine learning approach (tensorflow). Brain. 2018;5(04):2089–94.
21. Alsubai S, Khan HU, Alqahtani A, Sha M, Abbas S, Mohammad UG. Ensemble deep learning for brain tumor detection. Front Comput Neurosci. 2022;16:1005617. doi:10.3389/fncom.2022.1005617.
22. Gupta M, Sharma SK, Sampada GC. Classification of brain tumor images using CNN. Comput Intell Neurosci. 2023;2023:2002855. doi:10.1155/2023/2002855.
23. Ibrahim AU, Engo GM, Ame I, Nwekwo CW, Al-Turjman F. I-BrainNet: deep learning and Internet of Things (DL/IoT)-based framework for the classification of brain tumor. J Imaging Inform Med. 2025;38(6):3806–22. doi:10.1007/s10278-025-01470-1.
24. Sekhar A, Biswas S, Hazra R, Sunaniya AK, Mukherjee A, Yang L. Brain tumor classification using fine-tuned GoogLeNet features and machine learning algorithms: IoMT enabled CAD system. IEEE J Biomed Health Inform. 2022;26(3):983–91. doi:10.1109/JBHI.2021.3100758.
25. Khaliki MZ, Başarslan MS. Brain tumor detection from images and comparison with transfer learning methods and 3-layer CNN. Sci Rep. 2024;14(1):2664. doi:10.1038/s41598-024-52823-9.
26. Biswas A, Islam MS. Brain tumor types classification using K-means clustering and ANN approach. In: Proceedings of the 2021 2nd International Conference on Robotics, Electrical and Signal Processing Techniques (ICREST); 2021 Jan 5–7; Dhaka, Bangladesh. p. 654–8. doi:10.1109/icrest51555.2021.9331115.
27. Amin J, Anjum MA, Sharif M, Jabeen S, Kadry S, Moreno Ger P. A new model for brain tumor detection using ensemble transfer learning and quantum variational classifier. Comput Intell Neurosci. 2022;2022:3236305. doi:10.1155/2022/3236305.
28. Ibrahim AU, Nwaneri IO, Vubangsi M, Al-Turjman F. I-brainer: artificial intelligence/Internet of Things (AI/IoT)-powered detection of brain cancer. Curr Med Imag Former Curr Med Imag Rev. 2025;21:e15734056333393. doi:10.2174/0115734056333393250117164020.
29. Ain NU, Ali Khan S, Aladhadh S, Mir U, Ramzan M. Transformers meet CNNs: a comprehensive review and benchmarking of deep learning architectures for brain tumor classification in MRI. Comput Sci Rev. 2026;60:100897. doi:10.1016/j.cosrev.2026.100897.
30. Masmoudi Y, Ramzan M, Ali Khan S, Habib M. Optimal feature extraction and ulcer classification from WCE image data using deep learning. Soft Comput. 2022;26(16):7979–92. doi:10.1007/s00500-022-06900-8.
31. V NV, Manikandan MS, Gini R, Soman KP. A new framework to automatically select noise model for rician noise estimation in MR images. In: Proceedings of the 2012 International Conference on Advances in Computing and Communications; 2012 Aug 9–11; Cochin, India. p. 82–5. doi:10.1109/ICACC.2012.17.
32. Briganti G, Le Moine O. Artificial intelligence in medicine: today and tomorrow. Front Med. 2020;7:27. doi:10.3389/fmed.2020.00027.
33. Irkham I, Ibrahim AU, Nwekwo CW, Al-Turjman F, Hartati YW. Current technologies for detection of COVID-19: biosensors, artificial intelligence and Internet of medical things (IoMT): review. Sensors. 2023;23(1):426. doi:10.3390/s23010426.